Lateral Motion and Bending of Microtubules Studied with a New Single-Filament Tracking Routine in Living Cells

Carla Pallavicini,† Valeria Levi,‡¶ Diana E. Wetzler,‡¶ Juan F. Angiolini,‡ Lorena Benseñor,§¶ Marcelo A. Despósito,†¶ and Luciana Bruno†¶*
†Departamento de Física, Facultad de Ciencias Exactas y Naturales, and ‡Departamento de Química Biológica, Facultad de Ciencias Exactas y Naturales, Universidad de Buenos Aires, Buenos Aires, Argentina; §Fundación Instituto Leloir, Instituto de Investigaciones Bioquímicas de Buenos Aires-Consejo Nacional de Investigaciones Científicas y Técnicas, Buenos Aires, Argentina; and ¶Consejo Nacional de Investigaciones Científicas y Técnicas, Argentina

Supporting Material

1. Generation of simulated images

Simulated images were generated following the procedure described by Bicek et al (1) with some modifications. Briefly, the *x-y* coordinates of the microtubule were set numerically with computer decimal accuracy. Then, we used the *fspecial* command in Matlab to convolve the resulting image with a simulated point spread function similar to that obtained in our confocal microscope. The signal and background levels of the resulting images were set according to the specific simulation experiment. Then, the grid was coarse-grained to a grid size corresponding to 100 nm except where indicated and a random noise sorted from a Poisson distribution was added to each pixel of the simulated image. This procedure allows recovering simulated images that are similar to those collected in our confocal setup.

2. Simulation of filaments with thermal shapes

To simulate filaments with shapes following a thermal distribution, we sampled the mode amplitudes a_n from a normal distribution with variances given by Eq. 6.

For these simulations, we considered L = 8 μm (i.e., identical to the filament segments analyzed in the experiments), lp = 15 μm and $1< n < 1000$.

For each set of a_n, we computed $\theta(s)$ (Eq. 3) using 1 nm steps for *s* and recovered the coordinates *x* and *y* along the filament as (2):

$$x(\theta(s)) = \int_0^s \cos(\theta(s'))ds'$$

$$y(\theta(s)) = \int_0^s \sin(\theta(s'))ds'$$

Then, we simulated confocal images of these thermal filaments as described above. The S/N of the images was set to 10.

3. Tip-tracking routine

The tip-tracking routine starts when the program displays the first image of the loaded image stack. The user then selects in the image 2 initial positions; one located approximately on top of the tip and the other (auxiliary point) located on the filament at ~ 20 pixels from the tip. Then, the algorithm precisely relocates the *y*-coordinates of

these two points in the center of the MT using the same neural network interpolation routine described for the filament tracking routine.

These two initial points define a longitudinal axis placed at the center of the filament. We could verify that the intensity profiles along this axis followed a sigmoid-like distribution as expected; the *x*-coordinate of the tip is then computed as the position at which the sigmoid-like interpolation reaches half of its maximum value. To determine the *y*-coordinate of the tip, the program follows the procedure described for the filament tracking routine and uses a neural network interpolation to analyze the intensity profile perpendicular to the filament axis at the *x*-position previously determined for the tip.

The sub-pixel positions of the tip and the auxiliary point are recorded in the program and used as starting positions in the subsequent frame. The procedures described below are repeated to analyze the whole image stack.

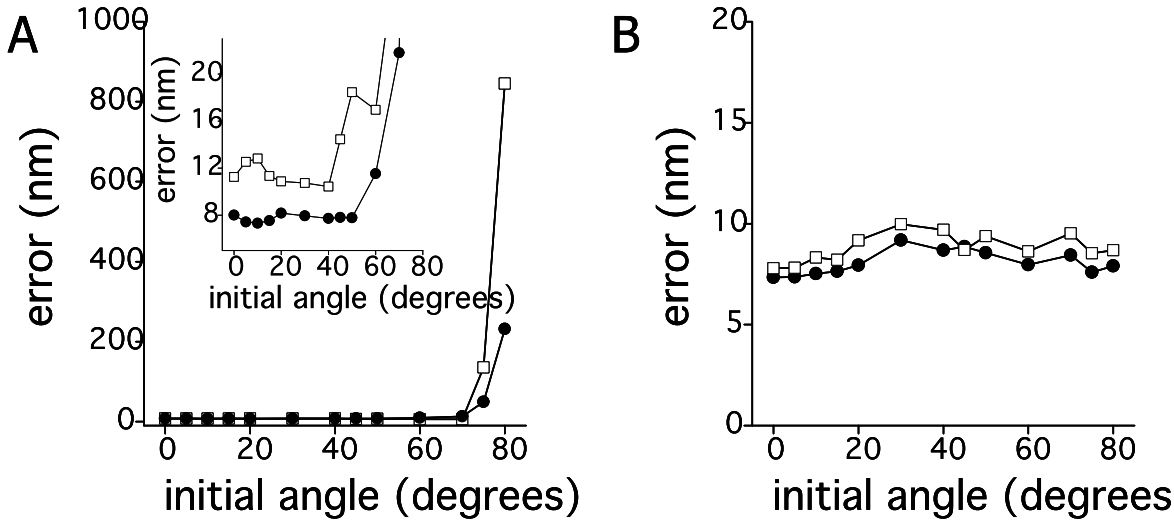

Supplementary Figure 1: Evaluation of image rotation on the algorithm performance. (A) We simulated a stack of 20 confocal images of a straight, fluorescent filament (S/N = 10) in an angle with respect to the *x* axis and calculated the error on the filament position determination (Eq. 5) as a function of the angle. Inset: zoom-in of the data corresponding to angles < 70^{o} (B) The same image-stacks were rotated to set the filament image parallel to the *x*-axis and the error on the filament position determination was calculated. The pixel sizes of the simulated images were 100 (●) or 200 nm (□).

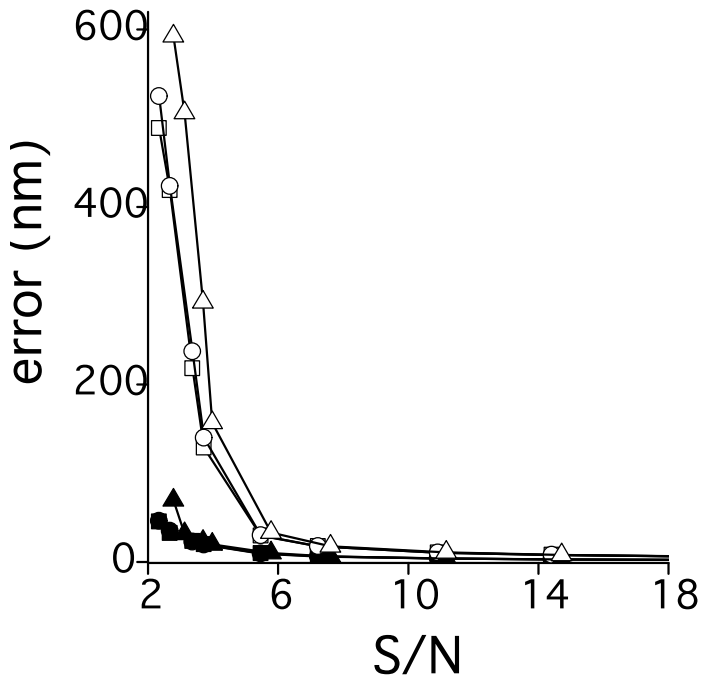

Supplementary Figure 2: Performance of the filament tracking algorithm in the presence of a linear-gradient background. We simulated a stack of 20 confocal images of a fluorescent filament with different S/N ratios as described before in the presence of a linear gradient background with slopes: 0 (■, □), 0.1 (●,○) and 0.2 (▲,△) counts/pixel. The simulated filament was tracked using the proposed neural network-based tracking routine (filled symbols) or a Gaussian deconvolution based algorithm (empty symbols) and the error on the filament localization was determined using Eq 5.

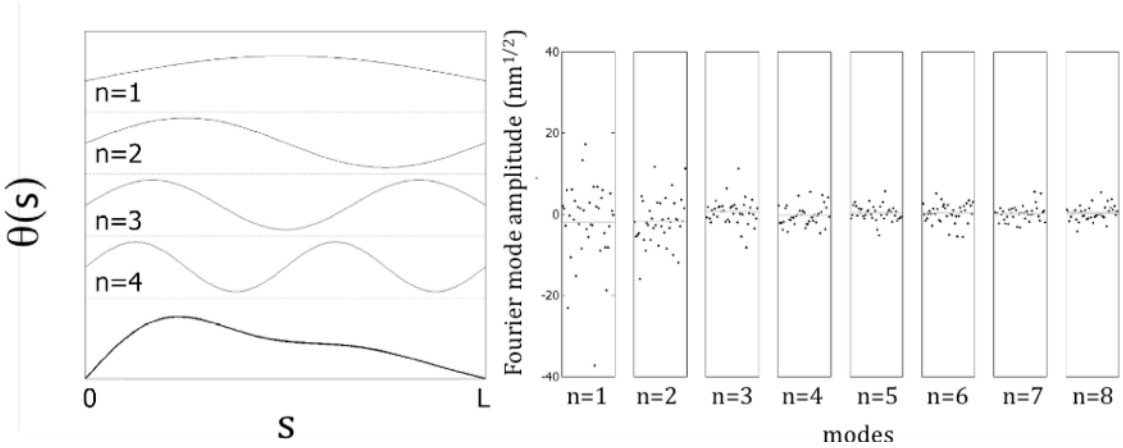

Supplementary Figure 3. Illustration of the Fourier decomposition of MT segments curvatures. (A) The curvature of a MT segment θ(s) was computed from the recovered (*x,y*) coordinates as explained in Materials and Methods. Briefly, θ(s) is the tangent angle of the recovered shape at each coordinate s along the filament. The lower panel shows a representative curvature θ(s) obtained with this procedure. θ(s) can be written as a sum of Fourier modes with amplitudes a_q and frequencies q_n that are integer multiples of the wave vector $q= \pi/L$, where L is the length of the segment. The first 4 modes are shown in this figure. (B) The boxes contain the amplitudes obtained for the first 8 modes of the Fourier decomposition corresponding to different filaments recovered in melanophore cells expressing XTP-GFP in control conditions. Each point represents the amplitude of a single filament.

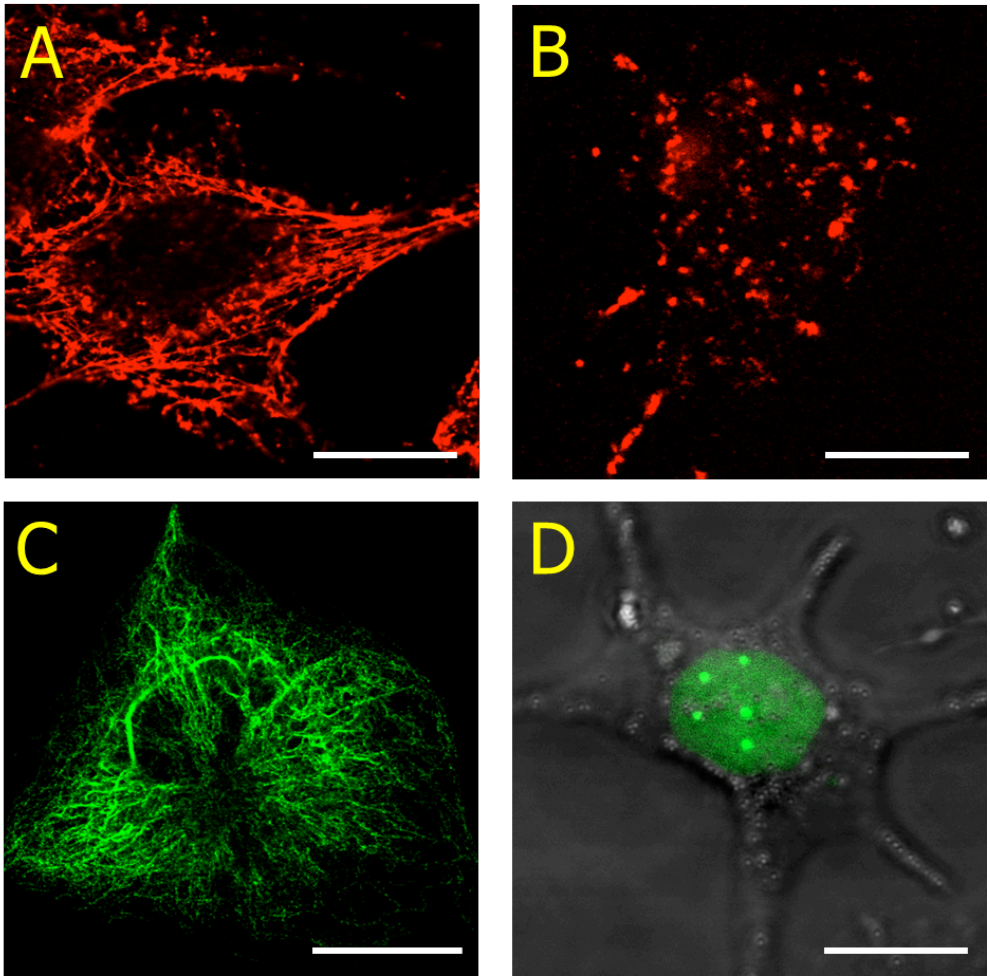

Supplementary Figure 4. Disruption of actin and vimentin networks. (A-B) Confocal images of control (A) or latrunculin-treated (B) cells fixed and labeled with rhodamine phalloidin following the manufacturer´s instructions (Invitrogen, Carlsbad, CA) to stain actin filaments. (C) Confocal images of melanophore cells transfected witch GFP-vimentin (C) and GFP-tagged dominant negative construct (D). In this last case, the image corresponds to the overlay of the fluorescence and phase contrast images to show the cell morphology. Scale bars, 20 μm.

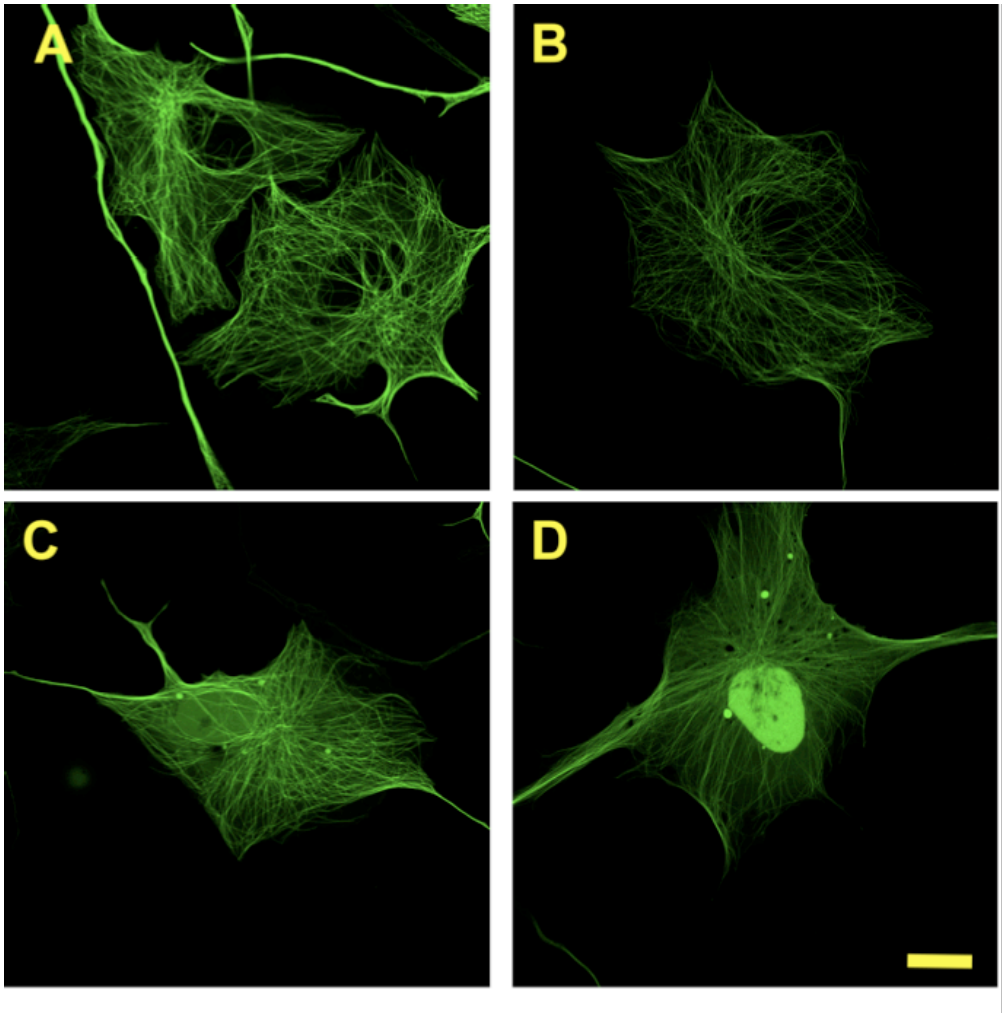

Supplementary Figure 5. ConfocaI images of melanophore cells expressing XTP-GFP in control conditions (A-B) or after transfection of a plasmid encoding the truncated version of vimentin-GFP that disrupt the endogenous intermediate filament network (C-D). Scale bar, 20 μm

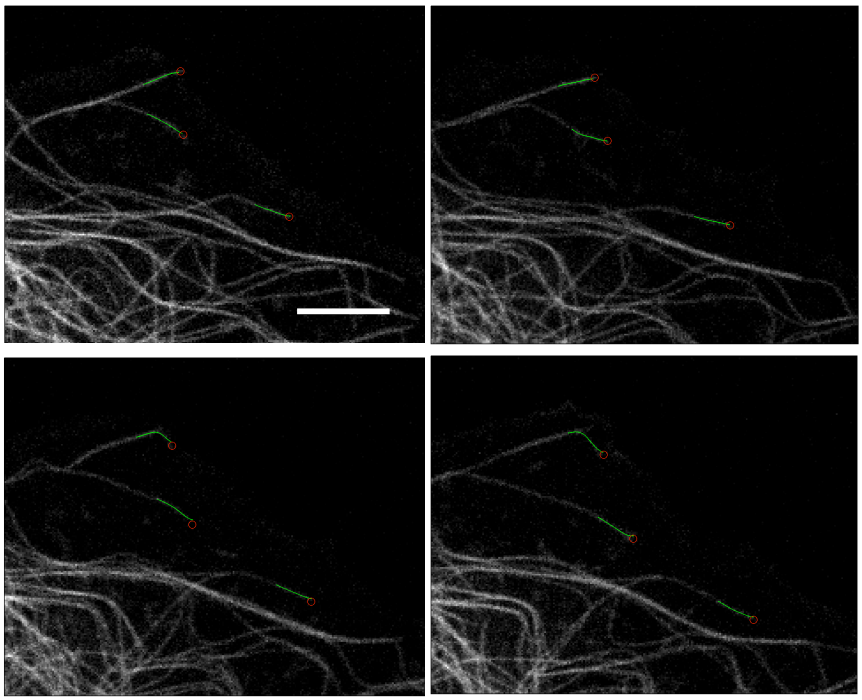

Supplementary Figure 6. Tracking microtubule tips in living cells. We acquired confocal images of melanophore cells expressing XTP-GFP as a function of time and used a combination of the tip-tracking and filament-tracking routines to follow the motion of microtubules plus-end regions. Representative frames obtained at 5, 25, 50 and 70s (top-left to bottom-right) The red circles show the position of the tips recovered in these images, the green line corresponds to the position of the plus-end region of these microtubules (segment size ~ 2 μm). Scale bar, 5 μm.

Supplementary Movie 1. Representative movie of a *Xenopus laevis* melanophore expressing XTP-EGFP. The confocal images were acquired at 0.17 frames/s and correspond to a region of ~71 x 71 μm^2 .

Supplementary references

1. Bicek, A. D., E. Tuzel, D. M. Kroll, and D. J. Odde. 2007. Analysis of microtubule curvature. Methods Cell Biol 83:237-268.
2. Gittes, F., E. Meyhofer, S. Baek, and J. Howard. 1996. Directional loading of the kinesin motor molecule as it buckles a microtubule. Biophys J 70:418-429.